HHS Public Access

Author manuscript

Neuron. Author manuscript; available in PMC 2017 February 03.

Published in final edited form as:

Neuron. 2016 February 3; 89(3): 521–535. doi:10.1016/j.neuron.2015.11.020.

Early somatostatin interneuron connectivity mediates the maturation of deep layer cortical circuits

Sebnem N. Tuncdemir[1], **Brie Wamsley**[1], **Floor J. Stam**[2], **Fumitaka Osakada**[2], **Martyn Goulding**[2], **Edward M. Callaway**[2], **Bernardo Rudy**[1], and **Gord Fishell**[1,*]

[1]NYU Neuroscience Institute and the Department of Neuroscience and Physiology, Smilow Research Center, New York University School of Medicine, 522 First Avenue, New York, NY 10016, USA

[2]Molecular Neurobiology Laboratory, The Salk Institute for Biological Studies, La Jolla, CA 92037, USA

[3]Systems Neurobiology Laboratories, The Salk Institute for Biological Studies, La Jolla, CA 92037, USA

Summary

The precise connectivity of somatostatin and parvalbumin cortical interneurons is generated during development. An understanding of how these interneuron classes incorporate into cortical circuitry is incomplete but essential to elucidate the roles they play during maturation. Here, we report that somatostatin interneurons in infragranular layers receive dense but transient innervation from thalamocortical afferents during the first postnatal week. During this period, parvalbumin interneurons and pyramidal neurons within the same layers receive weaker thalamocortical inputs; yet are strongly innervated by somatostatin interneurons. Further, upon disruption of the early (but not late) somatostatin interneuron network, the synaptic maturation of thalamocortical inputs onto parvalbumin interneurons is arrested. These results suggest that infragranular somatostatin interneurons exhibit a transient early synaptic connectivity that is essential for the establishment of thalamic feed-forward inhibition mediated by parvalbumin interneurons.

Introduction

GABAergic cortical interneurons represent a minority (~20%) of the neurons within the neocortex, but are required to dynamically sculpt activity within the cortex by virtue of their diverse anatomical, physiological and synaptic properties (Petilla Interneuron Nomenclature

*To whom correspondence should be directed: Gord Fishell: fisheg01@nyumc.org.

Author Contributions

S.N.T. performed all experiments and analysis except the synaptic puncta analyses performed by B.W. F.J.S. generated the conditional *Rosa-HTB* reporter mouse and F.O. provided the stock RV-mCherry and B7GG and BHK-EnvA, cell lines used to amplify and pseudotype the rabies virus. M.G., E.C, B.R., G.F. oversaw experiments, analysis and project direction. S.N.T. and G.F. planned and designed experiments and wrote the paper.

et al., 2008). Their generation, migration, and maturation is orchestrated by genetic and activity dependent programs (Kepecs and Fishell, 2014; Wonders and Anderson, 2006). Nonetheless, if we are to understand how interneurons assemble within developing neocortex and contribute to its maturation a better understanding of how they achieve their mature synaptic connectivity is needed.

During development, interneurons integrate into a six–layered neocortex that is assembled in an inside-out fashion. Early-born excitatory pyramidal neurons populate the infragranular (deep) layers, while later born pyramidal neurons (PN) are positioned in supragranular (superficial) layers (Angevine and Sidman, 1961). The assembly of cortical connectivity follows a similar pattern, beginning with deep cortical layer innervation at birth (P0), followed by the gradual acquisition of more superficially positioned topographic units by P8 (Minlebaev et al., 2011; Molnar et al., 2003). This process is facilitated by transient circuits involving early generated subplate neurons, which act as temporary conduits between the thalamus and other cortical or subcortical regions during the period when cortical synapses mature (Kanold and Luhmann, 2010). By late prenatal period, the earliest generated cohorts of interneurons are already positioned within the infragranular layers and have begun to establish their afferent and efferent connectivity (Miyoshi et al., 2007). However, whether they immediately integrate into their adult circuits or transiently form connectivity that aids in the establishment of mature synaptic wiring is unknown.

The two most prevalent early born interneuron populations are the low threshold-spiking somatostatin (SST) and fast-spiking parvalbumin (PV) interneurons, which are generated within the medial ganglionic eminence (MGE) (Rudy et al., 2011). PV and SST interneurons, in addition to sharing a common embryonic origin, express an overlapping set of transcription factors that control their differentiation, and positioning within cortical laminae (Bartolini et al., 2013; Batista-Brito and Fishell, 2009; Wonders and Anderson, 2006). Despite these commonalities, each cell class exhibits distinct patterns of synaptic specificity in mature cortical circuits. In the somatosensory barrel cortex, a large fraction of the SST interneurons target dendrites and provide feedback inhibition to local pyramidal neuron networks (Kapfer et al., 2007; Silberberg and Markram, 2007). By contrast, PV interneurons are strongly recruited by ascending sensory thalamic inputs, and form feed-forward perisomatic inhibition to the same cells that receive direct thalamic excitation (Cruikshank et al., 2007; Gabernet et al., 2005).

Considerable evidence suggests that the development of the PV interneuron innervation extends well into late postnatal stages and is regulated by sensory experience during critical periods of plasticity (Chattopadhyaya et al., 2004; Chittajallu and Isaac, 2010; Jiao et al., 2006; Morales et al., 2002). GABAergic synapses between PV interneurons, as well as those impinging upon pyramidal cells appear at the end of the first postnatal week concurrent with the appearance of excitatory inputs from pyramidal cells and thalamocortical afferents (Daw et al., 2007; Pangratz-Fuehrer and Hestrin, 2011). However, GABAergic synapses are present in the neocortex before synapses of PV interneurons appear to be functional (Agmon et al., 1996; Luhmann and Prince, 1991). This indicates that another source of presynaptic GABA must be present in the developing cortex and SST interneurons represent one source that could provide this innervation (Lazarus and Huang, 2011; Long et al., 2005; Takesian et

al., 2013). Consistent with this idea, the hippocampal network contains long range projecting SST cells that are present by P5 and particularly effective in supporting immature network synchronization (Bonifazi et al., 2009; Picardo et al., 2011). These 'hub' SST interneurons in the hippocampus precociously exhibit mature structural and functional properties and they share a common embryonic origin with neocortical SST interneurons. This raises the question as to whether cortical SST interneurons play a role in the functional maturation of neocortex.

To address whether SST interneurons dynamically modify their connectivity as neocortical development progresses, we examined if changes occur in their afferents and efferents during postnatal maturation. We found that during the first postnatal week, SST interneurons in infragranular layers receive denser thalamocortical (TC) inputs compared to more mature mice. By comparison, PV interneurons and pyramidal neurons in deep layers received weak TC inputs and are broadly recruited by SST interneurons in immature animals. Moreover, disruption of this early SST interneuron network resulted in defects in the TC innervation of infragranular PV interneurons. This indicates a selective requirement for early SST interneuron function for the maturation of PV interneuron input. Our work thus suggests that transient ascending activity relayed through SST interneurons operates in the establishment of inhibitory feed-forward circuits.

Results

SST interneuron afferents undergo reorganization during development

SST interneurons are among the earliest born cohort of MGE progenitors and invade the deep layers of the cortical plate as early as E17.5 (Miyoshi et al., 2007). To study their incorporatation into cortical circuits, we examined the development of their afferents using monosynaptic rabies tracing method (Wickersham et al., 2007). In young animals, we used a conditional *Rosa-HTB* (*HTB*: H, histone-tagged GFP; T, TVA receptor; B, rabies glycoprotein) reporter line (Li et al., 2013) in combination with a SST^{CRE} driver line (Taniguchi et al., 2011) to target rabies infection to SST interneurons and limit viral spread to first order presynaptic partners. At P1, we injected the infragranular layers of barrel somatosensory cortex (S1BC) with EnvA-pseudotyped G-deleted rabies virus encoding mCherry (EnvA+RV*dG*-mCh, henceforth called RV-mCh) and at P6 analyzed their monosynaptic inputs (n=5, Figure S1A). Because after P10 rabies glycoprotein levels from the Rosa-locus are insufficient to mediate synaptic transfer, we modified our approach to examine later developmental time points. Post-P10, the conditional *Rosa-TVA* reporter line (Seidler et al., 2008) was used to target RV-mCh infection into SST interneurons, complemented with a cre-dependent AAV helper virus that expressed the B19 rabies glycoprotein (Sun et al., 2014). The infragranular layers of S1BC was injected at P2 (n=2) or P15 (n=5) with AAV-hGFP-RG, followed 3–4 weeks later by RV-mCh injection into the same location. Analysis of the monosynaptic inputs to SST interneurons was done 5 days later (Figure S1B).

Monosynaptic labeling resulted in yellow cells (hGFP and mCh expression) that represent the SST starter cells, mCherry cells which are presynaptic to these starter cells, and hGFP positive SST cells that were not infected with RV-mCh (Figures 1A, B and insets). As

predicted, *cre* negative control animals showed no indication of RV-mCh infection at both ages (data not shown). Quantitative examination of every sixth (25-μm-thick) section indicated that the majority of the starter cells were localized to the L5 and L6 of the S1BC (Table S1), and a Pearson's chi-square test showed no correlation between developmental stage and laminar distribution of starter cells ($\chi^2(df = 3, N = 720) = 6.507$, $p = 0.0894$, Figure 1C).

At both postnatal ages, we observed extensive mCh labeling in trans-synaptically infected cells within a ~2mm wide area extending rostrocaudally in the ipsilateral neocortex with the highest density being around the injection site. At P6, both local and more distant cortical inputs predominantly originated from infragranular layers (Figures 1A, 1D, 1F). The majority of trans-synaptically labeled cells displayed tufted pyramidal cell morphologies with brightly labeled apical dendrites extending towards L1. Only a small portion of the presynaptic neurons expressed GABA (Figures 1D, S1C,D). Interestingly, SST interneurons in immature animals received afferents from several subcortical and cortical sources, the majority of which originated from the ventrobasal (VB, consisting of VPM and VPL) and posterior medial (PoM) nuclei of the thalamus (Figures 1G, I). Albeit in far sparser number, other regions that provided afferents included the ipsilateral motor cortex, the contralateral S1 and the nucleus basalis (Figures S1E–G).

Within the mature cortex the general pattern of SST interneuron afferents from deep cortical layers was conserved. In addition, mature SST interneurons received broad inputs from all cortical layers both proximal to the starter cells (50% of inputs originated from L5/6, 25% from L4, and 25% from L2/3 150 μm from the injection site, Figures 1B, F), as well as from more distant cortical regions (66% were in L5/6 and 30% in L2/3 300 μm from the injection site, Figures 1E, F). Consistent with the observed changes in intracortical afferents, a Pearson's chi square test showed that the laminar distribution of presynaptic neurons was significantly dependent on developmental stage (proximal inputs, $\chi^2(df = 4, N = 200) = 55.26$, $p < 0.0001$; distal inputs, $\chi^2(df = 4, N = 200) = 43.57$, $p < 0.0001$, Figure 1C). Despite the changes in the distribution of intracortical afferents in mature animals, the majority of afferent projecting cells had a pyramidal neuron morphology (Figure 1E) intermixed with a small percentage of GABAergic interneurons (p=0.2, t-test, Figures S1C, D). By contrast, we observed a dramatic decrease in the number of thalamic afferents compared to earlier time points, in particular within the VB and PoM nuclei (Figures 1H, I). When normalized to the number of starter cells in each brain, there was an ~4-fold reduction in the number of thalamic cells providing input to the SST population in older compared to younger mice, However, none of the other areas had any obvious developmental changes in the number of their projections to SST interneurons ($\chi^2(df = 4, N = 972) = 38.76$, $p < 0.0001$, Figures 1I, S1H–J). Taken together, with regard to local connectivity we observed a dramatic increase in the number of trans-synaptically labeled cells in the upper layers of the somatosensory cortex (Figure 1J), consistent with the 'inside-out patterning' model of cortical development. By contrast, the transient presence of a large number of somatosensory thalamic nuclei afferents to L5/6 SST interneurons was unanticipated (Figure 1J).

Changes in SST interneuron afferent connectivity do not reflect differential sampling of L5 and L6 populations at different ages

One possibility that could explain the developmental shift in afferent TC projections to SST interneurons is that the starter populations at the two ages examined were not identical. For instance, perhaps the number of early born SST interneuron population located in L5 and L6 at P6 was altered as a result of developmental cell death (Southwell et al., 2012). Alternatively, the later born (E11.5–E13.5) SST interneurons (Batista-Brito and Fishell, 2009) might "dilute out" the early born population and at later time-points. To examine these possibilities, we crossed the conditional reporter allele RCE^{EGFP} to SST^{CRE} mice and assessed cells born at E10.5 by intraperitoneally administering a saturating pulse of EdU. Our results indicate that both the total number of EGFP neurons (P6; L5, 162.81 ± 15.6; L6, 84.37 ± 16.7; P25; L5, 137.55 ± 12.7; L6, 104.24 ± 17.3, $p>0.1$, Figure 2B) and the number EdU-EGFP double-labeled cells in L5 and L6 of the S1BC at P6 brains and P25 were comparable (P6; L5, 52.17 ± 6; L6, 47.95 ± 6.9; P25; L5, 61.73 ± 7.3; L6, 57.23 ± 5.05, $p>0.1$, Figure2C). This argues against the selective loss or dilution of SST interneurons between the first and third postnatal weeks. In addition, the L5 and 6 SST interneuron population we sampled at P6 appeared similar to those seen in more mature SST interneurons (Xu et al., 2013), including L1 arborizing Martinotti types as well as neurons with axons within L1 and L4 (Figure 2D). This suggests that immature SST neurons within the cortex were distinct from the long-range projecting population in hippocampus (Bonifazi et al., 2009; Picardo et al., 2011). L5/6 SST neurons although still immature at P6 have already extended axons. Notably the SST^{Cre}-mediated recombination of the EGFP reporter, consistent with the previous reports (Hu et al., 2013; Neske et al., 2015), was not completely restricted to SST interneurons (Figure S2A). Nonetheless the fidelity was quite high: ~ 86% in L5 and 83% L6 at early postnatal ages and this did not change during development (84% in L5 and 89% L6, Figure S2B, C). Taken together, we conclude that the changes observed in SST interneuron afferent connectivity during development are not a result of changes in the interneuron populations examined. Even so, we sought to validate our anatomical findings by assessing the functional connectivity between the thalamus and L5/6 SST interneurons over this same time period.

Thalamocortical inputs onto immature SST interneurons are rapidly reduced after the first postnatal week

To test whether the changes in the anatomical pattern of connectivity revealed by the rabies tracing corresponds to functional connectivity of SST interneurons, we used channelrhodopsin (ChR2) to selectively activate TC axons in acute slices from $SST^{CRE};RCE^{EGFP}$ mice. We expressed mCh tagged ChR2 (mCh-ChR2) in TC afferents of immature (P5–7), and more mature (P17–21) animals by viral injections at embryonic (E14.5) or early postnatal (P2–3) ages, respectively (Figures S3A, S3B, Experimental Procedures). We were able to confine virus injection to the VB complex of the thalamus and did not observe retrograde labeling of cortical neurons (Figures 3A, S3C). We confirmed the efficiency of our injection strategies by recording postsynaptic responses in L4 spiny stellate neurons evoked by optogenetic stimulation of ChR2-expressing TC axons in the S1 cortex, 10–15 days after viral injections (Figure S3D). Brief pulses of light stimulation (470nm) evoked robust thalamic responses in L4 spiny stellate neurons (SSN) at P6 and P18. We also

applied TTX and 4-AP to allow for analysis of direct monosynaptic optical stimulation of thalamic terminals (Cruikshank et al., 2010; Petreanu et al., 2009). We then recorded from $EGFP^{-}$ expressing SST interneurons and nearby pyramidal neurons (PN) in the S1BC that were located near mCh^{+} TC arbors in lower half of L5 (adult L5B) and upper half of L6 (adult L6A) (Figures 3B, S3C, and L5/6 location of sampled cells are marked with dotted lines in Figure S2A). Optogenetic stimulation of TC fibers in the presence of TTX+4AP elicited monosynaptic EPSCs of larger amplitude in L5/6 SST interneurons than in PNs during first postnatal week (Figure 3Ci, D). By contrast, in P17–21 juvenile mice, we found that TC axons provided substantially weaker inputs to SST interneurons than nearby PNs (Figure 3Ciii,D). Importantly, optically evoked responses in L5/6 SST interneurons and PNs displayed onset latencies similar to those on L4 SSNs at each developmental time point, consistent with their monosynaptic origin (Figure S3E). TC excitatory inputs to SST interneurons were found to be significantly larger (155.1 ± 31.3 pA, n=13) than those received by PNs (51.22 ± 25 pA, n=13, $p<0.05$) during the first postnatal week. In contrast during the third postnatal week, TC-EPSCs in PNs (227.2 ± 32.42 pA, n=10) were always larger than in SST interneurons (56.8 ± 13.66 pA, n=13, $p<0.01$). Recordings in a current-clamp configuration also showed similar changes of TC evoked synaptic potentials in L5/6 SST interneurons relative to PNs during first and third postnatal weeks (Figures S4 B, D). Curiously, during first postnatal week, TC EPSPs recorded in L4 SSNs (12.72 ± 2.7 mV, n=7) was not statistically different than that of L5/6 SST interneurons (16 ± 1.7 mV, n=12, p=0.2, Mann-Whitney test).

Quantitatively, our results showed that the ratio of excitatory charge evoked by optogenetic thalamic stimulation was on average ~7 fold greater in SST interneurons compared to PNs during the initial stages of cortical development (Log2 normalized ratios of EPSQs shown in Figure 3E). However, by the beginning of second postnatal week the relative strength of these projections was substantially weaker onto SST interneurons relative to PNs (average EPSQ ~9 fold greater in PN compared to SST interneurons in second and third postnatal week). The observed differences are unlikely to be a result of differences in membrane properties or insufficient voltage clamping in more mature animals due to an increase in the cell surface area, as these changes appear concurrently in both cell types and likely exert similar effects on the TC input strengths at different developmental time points (Figures S3F–J, Table S2) (Zhang, 2004). Thus, our results suggest that SST interneuron functional maturation involves a transient period in which they are strongly activated by TC afferents compared to PNs. This synaptic connectivity is altered by the end of first postnatal week, resulting in reduced activation of these cells by the TC ascending pathways.

The underlying changes in TC evoked currents in SST interneurons could be due to a reduction in unitary conductance, synaptic connectivity (connection probability), or a combination of both mechanisms. To test for a decrease in the strength of unitary thalamic connections onto SST interneurons, we compared unitary synaptic events in genetically identified SST interneurons located in L5A/L6B in acute TC slices from the S1BC of immature (P3–P6) and adolescent (P18–25) mice (Figure 4A). We elicited postsynaptic responses by extracellular stimulation of thalamic axons exiting the VB nucleus just above threshold (50–500μA) to evoke EPSCs in about half of the trials, in an attempt to activate the axons of single thalamic relay neurons projecting to the postsynaptic SST interneuron (Gil et

al., 1999). The average amplitude of unitary thalamic EPSCs (excluding failures) was significantly larger in immature SST interneurons (54.89 ± 2.12 pA, n=15 out of 22 cells) than in those of older mice (39.15 ± 2.4 pA, n=12 out of 23 cells, $p<0.0001$, Figure 4D). The threshold for minimal stimulation amplitude was similar in immature animals compared to adolescent mice, (250 μA the example P4, P25 SST interneurons in Figure 4C), but the EPSC amplitude distributions tended to be smaller and less variable in older animals compared to those seen in immature animals. Evoked TC-EPSCs in immature SST interneurons had longer response delays than those recorded in older animals ($p<0.0001$, Kolmogorov-Smirnov test) but the averaged variance of delay to EPSC onset (jitter) was not significantly different between the two ages ($p=0.74$, Figures 4E,F). On the other hand, short-term plasticity (measured by paired-pulse ratio) or the kinetics of TC-EPSCs in immature and adolescent animals was not significantly different (Figures S4A–E).

The reduction of unitary EPSC amplitudes on SST interneurons in adolescent as compared to immature mice can only partially account for the decrease in thalamic inputs during development. Hence, we used immunohistochemical methods to label the synaptic contacts between thalamic afferents and SST interneurons to quantify synapse numbers (Eroglu et al., 2009). Specifically, we examined coronal brain sections from P5 and P30 SST^{CRE};$Ai9^{TdTomato}$ mice. We immunostained these sections for the presynaptic vesicular glutamate transporter 2 (Vglut2) to label thalamic axon terminals (Narboux-Neme et al., 2012), and the density of presynaptic puncta on the soma and proximal dendrites of SST interneurons was quantified. Our results illustrated a higher density of Vglut2 terminals terminate on P5 compared to P30 SST interneurons (Figures 4G, H). Both results indicate that over time the number of synaptic contacts between TC axons and SST interneurons are reduced and there is a small but significant decrease in the amplitude of the unitary thalamic EPSC. Taken together, these analyses independently validate the rabies-based retrograde monosynaptic circuit tracing results by showing that SST interneurons undergo a transient phase during development in which they receive denser inputs from somatosensory thalamic nuclei.

Intriguingly, during the period in which TC drive is reduced in SST interneurons, previous studies in barrel cortex have shown increased recruitment of L4 PV interneurons by thalamic afferents (Chittajallu and Isaac, 2010; Daw et al., 2007). Hence, we examined the strength of thalamic inputs onto L5B/L6A PV interneurons in comparison to that of SST interneurons in acute TC slices from the S1BC of immature mice (Figure S5A). We took advantage of $Lhx6^{EGFP}$ BAC transgenic mice, in which the majority of MGE-derived INs are labeled and breed this allele onto a compound $SST^{CRE};Ai9^{TdTomato}$ genetic background, allowing us to distinguish between SST (Red/Green$^+$) and PV (Green$^+$) interneurons (Figure S5B). This demonstrated that between P3–6 the average amplitude of unitary thalamic EPSCs (excluding failures) was significantly larger in immature SST interneurons (54.28 ± 1.82 pA) than nearby PV interneurons (38.18 ± 3.6 pA, $p<0.01$, Figures S5C, D). Evoked TC-EPSCs in immature PV interneurons had longer response delays than those recorded in SST interneurons ($p<0.0001$, Kolmogorov-Smirnov test) but the jitter of onset latency was not significantly different between two cell types ($p=0.16$, Figures S5E, F). On the other hand, TC-EPSC decay tau ($p=0.01$) and rise times ($p=0.02$) displayed small but statistically significant shorter time courses of response in PV interneurons compared to that of SST

interneurons (Figures S5G–I), while paired-pulse ratios were not significantly different at thalamic synapses in both immature L5B/6A interneurons. (Figures S5J, K). Moreover, PV and SST interneurons in immature animals had very similar responses to incremental step current injections (Figures S5K–M, Table S2), suggesting that intrinsic membrane properties of infragranular interneurons cannot account for differences in the strength of TC inputs evoked at immature ages. Instead, our results provide evidence for a preferential targeting of SST interneurons by TC axons in the immature somatosensory cortex.

Immature SST interneurons broadly innervate deep cortical layers

In the adult neocortex, SST interneurons in L5 and L6 preferentially innervate PNs (Kapfer et al., 2007; Pfeffer et al., 2013; Silberberg and Markram, 2007). To examine functional outputs of SST interneurons in the transient phase during which they receive stronger thalamic innervation, we used ChR2 to selectively activate SST interneurons in immature or older cortices and measured the postsynaptic responses in PV interneurons and PNs in L5B/L6A of S1BC (Figure 5A). ChR2 was targeted to SST interneurons by crossing the conditional $Ai32^{ChR2\text{-}EYFP}$ reporter line with $SST^{CRE};Lhx6^{EGFP}$ compound mice. In a subset of recordings, we injected an AAV-flex-hChR2.mCherry into S1BC of $SST^{CRE};Lhx6^{EGFP}$ mice at P1 to selectively activate SST interneurons within L5 and L6 (Figure 5D). In both instances, we found that light stimulation reliably evoked action potential firing in SST interneurons at all time-points examined (Figure 5B). Subsequently, we recorded synaptic currents in EGFP positive PV interneurons and adjacent pyramidal cells in at 0mV holding potential and in the presence of NBQX (10μM) and DAP-5 (25μM) to block all cortical excitation (Figures 5C, E). In immature animals, optogenetic stimulation of SST interneurons resulted in postsynaptic currents in L5/6 PV interneurons that were similar in amplitude to that of adjacently localized PNs (PV 93.78 ± 12.5 pA, n=5 transgenic-filled circles, n=6 virus induced-open circles; PN 126.9 ± 20.12 pA, n=6 transgenic-filled circles, n=5 virus induced-open circles p=0.26) (Figure 5F). In contrast, postsynaptic responses in older animals were preferentially seen in PNs compared to nearby PV interneurons (PV interneurons 56.44 ± 12.1 pA, n=5 transgenic, PN 224.1 ± 37.5 pA, n=6 transgenic, $p<0.005$). Delays of evoked SST-PSCs were not significantly different among simultaneously recorded cell pairs at both ages (Figure 5G). Taken together, our observations provide anatomical evidence that the disynaptic feedback circuit motif among deep layer SST interneurons and local PNs is formed gradually during early postnatal ages. Surprisingly at early postnatal ages, SST interneurons act as an intermediate relay for TC afferent outputs to PV interneurons and PNs, prior to when TC afferents target these latter populations.

Disruption of the SST interneuron network during early development leads to an arrest in PV interneuron maturation

We then sought to address whether this transient phase of SST interneuron connectivity might have lasting importance for cortical development by disrupting the early born SST interneuron population. We ablated SST interneurons using conditional *Rosa-DTA* mice that express diphtheria toxin A selectively in SST interneurons beginning around E13. The number of SST expressing cells in $SST^{CRE};$ *Rosa-DTA* animals was decreased to ~50% of controls within L5/6 as confirmed by SST-immunocytochemistry performed at P6 (Figures

6A,B). The number of cells was not reduced further at P11 (Figure S6A). Intriguingly, evoked TC unitary responses (Figure 6C) in PV interneurons recorded on P10–15 had synaptic responses reminiscent of those seen in more immature cells (Figure 6D). The evoked TC-EPSC amplitude in PV interneurons was reduced ($p<0.05$) and the averaged onset latency was increased ($p<0.01$, Figure E) compared to controls. Although the decay tau or short-term synaptic dynamics of the TC-EPSCs were not significantly altered (Figures S6C–E), the events displayed significantly longer rise times ($p<0.05$, Figure 6E), with only a small reduction in the frequency of PV interneuron firing at suprathreshold current injections ($p>0.05$, Figures S6F,G) likely reflecting the partial removal of the L5/6 SST interneuron population. These defects in thalamic input on PV interneurons occurred without apparent changes in the arborization of thalamic fibers within the input layers of S1BC or significant changes in direct thalamic inputs onto PNs (Figures S6H–J). However, the reduction of TC drive on PV interneurons was reflected in their reduced disynaptic feed-forward inhibitory response to TC stimulation (Figure S6L). Consequently, the temporal integration window (IW) recorded in PNs (Kruglikov and Rudy, 2008), reflecting the latency between the onset of TC excitation of PNs and the onset of feed-forward inhibition, was significantly prolonged ($p<0.05$, Figures 6F,G). This indicates a requirement of SST interneurons for infragranular PV interneurons to develop feed-forward TC circuits.

To independently test the requirement of SST interneurons during development, we took advantage of a previously characterized mouse model in which cortical SST interneurons fail to mature properly during development upon the removal of *Satb1 (special AT-rich binding protein)* specifically from SST interneurons (Close et al., 2012). As *Satb1* expression is restricted to dorsal telencephalon (Figure S7A, Website: ©2013 Allen Institute for Brain Science.), this mouse model allows us to test the requirement of cortical SST interneurons. In addition, we have previously shown that in $SST^{CRE};Satb1^{C/C}$ mutant animals, the number of SST interneuron population is largely intact at P5 compared with controls ($SST^{CRE};Satb1^{C/+}$) (Close et al., 2012). However, *Satb1* mutant SST interneurons received significantly reduced excitatory synapses, as assessed by Vglut2 and Vglut1 puncta density, at a time that control SST populations display transient synaptic connectivity (Figures 7A,B). *Satb1* loss of function subsequently results in a 40% reduction in SST interneuron population at P10 and a further reduction to 60% by P21 (Close et al., 2012). In $SST^{CRE};Satb1^{C/C}$ mutant animals, the evoked minimal TC input on EGFP-expressing ($Lhx6^{EGFP}$) PV interneurons on the second postnatal week (P10–14) had reduced EPSC amplitude ($p<0.05$) and increased averaged onset latency ($p<0.05$) with slower synaptic kinetics ($p<0.01$, Figures 7C–E), compared to PV interneurons in $SST^{CRE};Satb1^{C/+}$ control animals. Similar to the DTA depletion experiments, short-term synaptic dynamics of the TC-EPSCs in PV interneurons were not significantly altered (Figure S7D, E). In addition, although there were no apparent changes in direct TC inputs onto PNs (Figure S7H–J), reduced disynaptic feed-forward inhibitory responses to TC stimulation (Figure S7K) were reflected in significantly prolonged temporal IW in PNs ($p<0.05$, Figure 7F,G). These results indicate that SST interneurons promote the integration of PV interneurons into TC circuits by facilitating their TC synaptic maturation.

In order to show that these defects specifically reflect an early requirement of SST interneurons, we selectively depleted SST neurons by inducing diphtheria toxin receptor

(DTR) expression after the first postnatal week. We unilaterally injected an AAV-flex-DTR.GFP virus into the S1BC of $SST^{CRE};Ai9^{TdTomato}$ animals at P1, and administered diphtheria toxin (DT; 400ng) at P8 (Azim et al., 2014). The number of tdTomato expressing cells in the virus injected hemispheres was on average decreased to ~70% of the contralateral hemisphere at P15 (Figure 8A,B). Yet, evoked TC unitary responses (Figure 8C) in PV interneurons recorded on P13–17 had synaptic responses similar to those recorded in control hemispheres ($p>0.2$, Figure 8D, E). Furthermore, neither disynaptic inhibitory responses in PNs (Figure 8F) nor the resulting IW ($p=0.22$, Figure 8G, H) were altered in the absence of SST interneurons. Together these results indicate that proper establishment of thalamic inputs on PV interneurons and feed-forward inhibitory responses in PNs are dependent on transient SST interneuron connectivity, present only during first postnatal week.

Finally, we tested whether disrupting outputs of SST interneurons during first postnatal week leads to defects in TC inputs onto PV interneurons, comparable to those seen in SST ablation and *Satb1* loss of function experiments. Genetic manipulations of SST interneurons' synaptic outputs were achieved by using conditional expression of tetanus toxin light chain subunit (TeNT), which attenuates evoked vesicular synaptic transmission (Zhang et al., 2008) or conditional ablation of GABA transporter *Vgat* from SST cells, which is required for presynaptic release of GABA (Tong et al., 2008). In SST^{CRE};Rosa-TeNT mutant animals, the evoked TC unitary responses in PV interneurons had synaptic responses similar to those recorded in control (SST^{CRE}) animals (PVEPSC: $p=0.6$, PVLatency: $p= 0.3$, PVRise time: $p= 0.3$, Figure S8 A–C). Furthermore, disynaptic inhibitory responses in PNs or the resulting IW (mutant, n=4, control n=5, PNIW: $p=0.7$, Figure S8D) were not altered in the absence of evoked vesicular release from SST interneurons. Interestingly, we observed a partial disruption of PV synaptic development in heterozygous $SST^{CRE};Vgat^{C/+}$ animals compared to controls (SST^{CRE}). Evoked minimal TC input on PV interneurons had reduced EPSC amplitude ($p<0.05$) and prolonged averaged onset latency ($p<0.05$, Figure S8A, B) with no significant changes in rise time of PV-EPSCs in heterozygous $SST^{CRE};Vgat^{C/+}$ mutants, compared to PV interneurons in controls ($p=0.4$, Figure S8C). In addition, temporal IW in mutant PNs was significantly prolonged compared to controls ($p<0.01$, Figure S8D). We have also analyzed evoked unitary TC events in SST^{CRE};Rosa-TeTN; $Vgat^{C/+}$compound mutant mice and observed defects similar to the SST^{CRE}; $Vgat^{C/+}$ mice (Figure S8). This suggests that the spontaneous vesicular GABA diffusion into the extracellular space, but not evoked synaptic transmission from SST interneurons is required for the synaptic development of PV interneurons.

Discussion

The mechanisms responsible for generating the remarkable precision of cortical interneuron connectivity during development remain poorly understood. It has been suggested that transient scaffolds provide versatile strategies for the construction of complex architectures (Bonifazi et al., 2009; Kanold and Luhmann, 2010). Here, we provide evidence that SST interneurons within the infragranular layers act as a transient intermediate relay between the thalamus and PV interneurons and PNs and contribute to the assembly of infragranular cortical networks. Moreover, disruption of this early SST interneuron network resulted in an

arrest in the maturation of the TC innervation of PV interneurons and hence the ability of the latter to function effectively.

Early born SST interneurons function as a pioneer population in nascent cortical networks

The earliest cohorts of SST interneurons, which migrate into the infragranular layers of the cortical plate by P0, represent the first interneuron population to integrate and function within the neocortex (Miyoshi et al., 2007; Miyoshi and Fishell, 2011). Here, we examined whether they share similar properties with previously identified pioneer populations, such as subplate neurons in the neocortex (Finney et al., 1998; Hanganu et al., 2002) and hub neurons in the hippocampus (Bonifazi et al., 2009; Picardo et al., 2011). To our surprise, despite their common embryonic origin and immunohistochemical properties, the earliest born SST interneurons are quite distinct from other pioneer populations. We found that the majority of the early SST interneurons become localized to layers 5 and 6, persist throughout development, and have structural and functional characteristics consistent with that seen in adult cortical SST interneurons. Moreover, unlike hippocampal “hub” cells, the L5/6 SST interneurons do not form dense, long-range projections. Rather, these immature SST cells receive dense transient thalamic input and provide efferent connections to PN and PV cINs during the first postnatal week; yet, they ultimately develop into the well-described L5/6 SST interneuron population. Taken together, our results suggest that while L5/6 SST interneurons begin to establish their mature character upon reaching the cortex, they concurrently play an unanticipated developmental role in the assembly of infragranular cortex.

Previous work by Sanes and colleagues has shown that LTS-SST interneurons in the L4 of gerbil auditory cortex display a developmental decrease in thalamic evoked synaptic potentials, in contrast to the developmental increase in thalamic synaptic potentials evoked in FS-PV interneurons (Takesian et al., 2013). Here, our monosynaptic rabies tracing (Figure 1), as well as physiological and anatomical examination of synapses (Figure 3,4) in L5/6 of mouse S1BC are consistent with this and indicate that the strength of the thalamic input onto SST interneurons diminishes by the beginning of the second postnatal week. These changes do not appear to be attributable to differences in presynaptic release probability or postsynaptic receptor composition (Figure S5) but could arise from elimination of TC inputs or disassembly of individual synaptic contacts (Goda and Davis, 2003). While the molecular and cellular signals that regulate pruning remain to be determined, they potentially involve developmental changes in trans-synaptic interactions between SST interneurons and presynaptic TC afferents (Williams et al., 2010).

We also demonstrate that the SST interneuron efferents dramatically alter their relative strength while maintaining their target specificity. In both immature and mature brains, L5/6 SST interneurons maintain projections to PNs and PV interneurons within the same layer (Figure 5). While at P5–7 the strength of SST interneuron synapses onto PV interneurons versus PNs are not significantly different, by the third postnatal week the connections between SST interneurons and PNs are significantly larger than those with PV interneurons. Although we do not have a clear understanding of the physiological impact of GABA released from SST interneurons onto their targets in the immature brain, GABAergic

signaling in the developing cortex has important functional consequences for cortical neuron development (Owens and Kriegstein, 2002; Represa and Ben-Ari, 2005). However at present, the precise source of GABA in the developing cortex to mediate these events remains unknown with one potential source being the local SST interneurons.

SST interneurons are essential for maturation of thalamic synapses on PV interneurons

We used three independent and complementary approaches to assess for a possible role of SST interneurons for the assembly of infragranular circuits during the first postnatal week. We observed that reducing the number of SST interneurons or their excitatory inputs during early (Figures 6,7), but not late (Figure 8) developmental stages cause significant defects in the establishment of thalamic afferents onto PV interneurons, as indicated by a reduction in their EPSC amplitude, prolonged latency, and slower kinetics. By contrast, TC inputs to L5/6 PNs remained largely unaffected; yet, evoked TC-mediated inhibition onto PNs is significantly reduced. Selectivity of SST interneuron function for TC synaptic development of PV interneurons is likely important for the maturation of cortical feed-forward inhibitory networks. We propose that the cross talk between the two subtypes of interneurons derived from a common embryonic origin is facilitated by the similarity of their migratory routes or transcriptional profiles (Bartolini et al., 2013; Batista-Brito and Fishell, 2009; Wonders and Anderson, 2006), and in turn is functionally important for the synaptic maturation of PV interneurons.

Our results indicate that the protracted development of thalamic-initiated feed-forward inhibition mediated by L5/6 PV interneurons (Beierlein and Connors, 2002; Cruikshank et al., 2010) is dependent on developmental interactions with SST interneurons. Despite demonstrating a clear requirement for SST cells in these events, understanding the precise role of their synaptic outputs in this process will require further investigation (Figure S8). Our observations portend that the early-appearing projections from SST cells onto PV interneurons in L5/6 could act as a transient functional relay between thalamus and PV interneurons. Nevertheless, blockade of evoked vesicular release from SST interneurons (by expressing tetanus toxin light chain) during their transient connectivity phase did not lead to defects in TC connectivity of PV interneurons (Figure S8). By contrast, reducing GABA within SST presynaptic sites by heterozygous *Vgat* removal during this same period partially phenocopied the affects on PV interneuron development seen when SST interneurons are ablated or genetically perturbed. Indeed, in agreement with the prominent requirement of GABAergic transmission for synaptic maturation of interneurons (Deidda et al., 2015; Sauer and Bartos, 2010), spontaneous GABA released from SST interneurons may tonically activate PV interneurons to promote their TC synapse development (Figure S8). Alternatively, SST interneurons may act as a postsynaptic placeholder for the TC afferents during first postnatal week, providing trophic support for the TC synaptic targeting of PV interneurons. Curiously, we observed that TC-EPSCs evoked in immature PV cells as compared to SST interneurons (Figure S5C, E) were smaller and had a longer latency of unitary discharge and this may indicate that distinct TC afferent fibers or synapses target different interneurons during initial stages of synapse formation. The exuberant TC targeting of SST interneurons before the onset of active sensory processing could allow them to act as necessary place holders for TC fibers until experience dependent *de novo* synapse formation

or potentiation of immature TC synapses to PV interneurons can selectively become established (Kanold and Luhmann, 2010; Takesian et al., 2013).

On a broader scale, in the future it will be interesting to explore whether SST interneurons in L4 or L2/3 of the somatosensory barrel cortex undergo similar changes during development in their synaptic connectivity or in the facilitation of the synaptic maturation of PV interneurons in those layers. For instance, the increased recruitment of L5/6 PV interneurons by TC afferents between P6 and P11 (Figures 6, S6) is reminiscent of the development of feed-forward inhibition in S1BC L4 circuits (Daw et al., 2007). Although increased recruitment of TC input on L4 PV interneurons is largely regulated by whisker experience via a presynaptic mechanism involving an increase in release probability (Chittajallu and Isaac, 2010), it remains to be investigated whether L4 SST interneurons may also facilitate TC synaptic maturation of L4 PV interneurons. If so, given the inside-out maturation of cortical layers, it is possible that consistent with their later birth (Miyoshi and Fishell, 2011) that in a stepwise manner they use similar mechanisms to promote circuit maturation. However, the possibility that all SST interneurons are all equivalent should be considered with caution, as previous work has shown that considerable heterogeneity among this population exists (Xu et al., 2013). In the mature somatosensory cortex, the majority of L4 SST interneurons belong to the so called “X94 class” and possess functional, morphological and synaptic connectivity profiles distinct from those seen in L2/3 and L5/6 SST cells (Ma et al., 2006; Xu et al., 2013). As such, due to the differences in the developmental time they arrive into the network and their synaptic connections, this population could potentially have profound differences both in their developmental integration to L4 circuits and their functional contribution to the maturation of those circuits.

In sum, our results complement previous work examining global organizers that orchestrate the assembly of excitatory circuits (Cossart, 2014; Kanold and Luhmann, 2010; Molnar and Clowry, 2012) by providing new insight into mechanisms by which inhibition is established in the cortex. Given that developmental insults to interneurons (PV interneurons in particular) are implicated as the underlying etiology of psychiatric disease (Karayannis et al., 2014; Marin, 2012; Owen et al., 2013), our results likely have particular importance. Specifically, they reveal the unanticipated development cooperation between SST and PV interneurons. As such, understanding how defects in PV interneurons manifest in psychiatric disease needs to consider their transient developmental dependency on early born SST interneurons.

Experimental procedures

All experimental procedures were conducted in accordance with the National Institutes of Health guidelines and were approved by the Institutional Animal Care and Use Committee of the NYU School of Medicine.

Mouse Strains

Generation and genotyping of *SST*^{CRE}, *Rosa-HTB*, *Rosa-TVA*, *RCE*^{EGFP} (Sousa et al., 2009), *Lhx6*^{EGFP}, *Rosa-Ai9*^{tdTomato}, *Rosa-Ai32*^{ChR2}, *Rosa-DTA*, *Satb1* conditional, Rosa-TeNT, Vgat conditional mouse strains have been described previously, see supplemental

experimental procedures. All mouse strains were maintained on a mixed background (Swiss Webster and C57/B16). The day of plug is considered as E0.5, the day of birth is considered P0.

Virus injections

Rabies virus was produced in B7GG cells stably expressing G protein for complementation, BHK-EnvA cells to produce EnvA-G protein pseudotyped viruses, and HEK293t and HEK293-TVA cells to determine viral titers as described previously (Osakada et al., 2011; Wickersham et al., 2007). Helper adeno-associated virus (100nL) carrying fusion gene for Rabies glycoprotein B19 (*AAV1/2.EF1a.FLEX.hGFP.B19G*; Gene Transfer, Targeting and Therapeutics Core, Salk Institute) was delivered as described previously (Owen et al., 2013). A detailed description of ultrasound backscatter-guided injection of AAV suspension has been described elsewhere (Nery et al., 2002). 25nL of *AAV2/1.CAG.hChR2(H134R)-mCherry.WPRE.SV40* (Addgene20938M, Upenn Vector Core) was injected unilaterally into VB thalamic complex. 100nL *of AAV2/1.Flex.EF1a.hChR2(H134R)-mCherry.WPRE.SV40* (Addgene20297, Upenn Vector Core) and *AAV2/1-Flex.DTR.GFP* (gift from T. Jessel) into cortex at P0-2 (see the Supplemental Experimental Procedures).

Immunohistochemistry

Procedures for immunohistochemistry have been previously described (Tuncdemir et al., 2015). Fluorescent images were captured using a fluroscence microscope (Axioscope A1, Zeiss) with an attached cooled-CCD camera (Princeton Scientific Instruments, NJ) using Metamorph software (Universal imaging, Downingtown, Pennsylvania). See the Supplemental Experimental Procedures for more detail on immunohistochemistry analyses.

Electrophysiology and analysis

Whole-cell patch-clamp recordings were obtained from EGFP, tdTomato expressing interneurons or non-fluorescent pyramidal shaped neurons that were located adjacent to the sampled interneuron from coronal (300μm) or thalamocortical slices (350 μm thick in immature animals, 400 μm in mature) in primary somatosensory cortex prepared as in (Kruglikov and Rudy, 2008) (see the Supplemental Experimental Procedures). Data were collected using a Multiclamp 700B amplifier (Molecular Devices), digitally sampled at 20 kHz and low-pass filtered at 5 kHz (Digidata 1440A, Molecular Devices), pClamp 10 software was used for data acquisition. Whole-cell voltage clamp holding potentials were −65mV for testing excitatory postsynaptic currents, 0mV for inhibitory postsynaptic currents, −45mV to obtain EPSC/IPSC sequences. To activate thalamic afferents, extracellular stimuli were delivered using tungsten bipolar stimulating electrode placed on axons exiting VB, the range of stimulation intensities were 20–500 μA. Photostimuli were produced by a blue light source (Mightex BioLED Light Source, 470nm) to stimulate ChR2 expressing fibers, mounted on the microscope in place of the binoculars and delivered through a 40X water immersion objective. Light pulses were 5 ms in duration (unless otherwise indicated) with a power of approximately 0.5mW per mm^2. Data analysis was performed off-line using the Clampfit (Molecular Devices), Prism 5 (GraphPad Software), and Microsoft Excel.

Statistical analyses

Data is presented throughout as the mean ± standard error of the mean (SEM). Significance level was selected as 0.05. All statistical comparisons are non-parametric (two-sided). Specific statistical analyses and sample sizes are notified within the figure legends. Statistical significance was expressed in the graphs in the following manner: * $p<0.05$, ** $p<0.01$, *** $p<0.001$ in the graphs.

Supplementary Material

Refer to Web version on PubMed Central for supplementary material.

Acknowledgments

We are grateful to Richard Tsien, Michael Long and members of the Fishell and Rudy labs for critical scientific discussions and comments on the manuscript. We thank Jiwon Choi for *AAV-EF1α-FLEX-hGFP-B19G* and Tom Jessell for *AAV-Flex-DTR-GFP* constructs. We thank Lihong Yin, Jiali Deng, and Jisen Dai for technical assistance. Research in the Fishell lab is supported by NIH (NS 081297, MH095147, P01NS074972) and the Simons Foundation. Research in the Rudy lab is supported by NIH (RO1NS30989, P01NS074972). Research in the Callaway lab is supported by NIH (EY022577, MH0639123) and the Gatsby Charitable Foundation.

References

Agmon A, Hollrigel G, O'Dowd DK. Functional GABAergic synaptic connection in neonatal mouse barrel cortex. J Neurosci. 1996; 16:4684–4695. [PubMed: 8764656]

Angevine JB Jr, Sidman RL. Autoradiographic study of cell migration during histogenesis of cerebral cortex in the mouse. Nature. 1961; 192:766–768. [PubMed: 17533671]

Azim E, Jiang J, Alstermark B, Jessell TM. Skilled reaching relies on a V2a propriospinal internal copy circuit. Nature. 2014; 508:357–363. [PubMed: 24487617]

Bartolini G, Ciceri G, Marin O. Integration of GABAergic interneurons into cortical cell assemblies: lessons from embryos and adults. Neuron. 2013; 79:849–864. [PubMed: 24012001]

Batista-Brito R, Fishell G. The developmental integration of cortical interneurons into a functional network. Curr Top Dev Biol. 2009; 87:81–118. [PubMed: 19427517]

Beierlein M, Connors BW. Short-term dynamics of thalamocortical and intracortical synapses onto layer 6 neurons in neocortex. Journal of neurophysiology. 2002; 88:1924–1932. [PubMed: 12364518]

Bonifazi P, Goldin M, Picardo MA, Jorquera I, Cattani A, Bianconi G, Represa A, Ben-Ari Y, Cossart R. GABAergic hub neurons orchestrate synchrony in developing hippocampal networks. Science. 2009; 326:1419–1424. [PubMed: 19965761]

Chattopadhyaya B, Di Cristo G, Higashiyama H, Knott GW, Kuhlman SJ, Welker E, Huang ZJ. Experience and activity-dependent maturation of perisomatic GABAergic innervation in primary visual cortex during a postnatal critical period. The Journal of neuroscience: the official journal of the Society for Neuroscience. 2004; 24:9598–9611. [PubMed: 15509747]

Chittajallu R, Isaac JT. Emergence of cortical inhibition by coordinated sensory-driven plasticity at distinct synaptic loci. Nature neuroscience. 2010; 13:1240–1248. [PubMed: 20871602]

Close J, Xu H, De Marco Garcia N, Batista-Brito R, Rossignol E, Rudy B, Fishell G. Satb1 is an activity-modulated transcription factor required for the terminal differentiation and connectivity of medial ganglionic eminence-derived cortical interneurons. J Neurosci. 2012; 32:17690–17705. [PubMed: 23223290]

Cossart R. Operational hub cells: a morpho-physiologically diverse class of GABAergic neurons united by a common function. Current opinion in neurobiology. 2014; 26:51–56. [PubMed: 24650504]

Cruikshank SJ, Lewis TJ, Connors BW. Synaptic basis for intense thalamocortical activation of feedforward inhibitory cells in neocortex. Nat Neurosci. 2007; 10:462–468. [PubMed: 17334362]

Cruikshank SJ, Urabe H, Nurmikko AV, Connors BW. Pathway-specific feedforward circuits between thalamus and neocortex revealed by selective optical stimulation of axons. Neuron. 2010; 65:230–245. [PubMed: 20152129]

Daw MI, Ashby MC, Isaac JT. Coordinated developmental recruitment of latent fast spiking interneurons in layer IV barrel cortex. Nature neuroscience. 2007; 10:453–461. [PubMed: 17351636]

Deidda G, Allegra M, Cerri C, Naskar S, Bony G, Zunino G, Bozzi Y, Caleo M, Cancedda L. Early depolarizing GABA controls critical-period plasticity in the rat visual cortex. Nat Neurosci. 2015; 18:87–96. [PubMed: 25485756]

Eroglu C, Allen NJ, Susman MW, O'Rourke NA, Park CY, Ozkan E, Chakraborty C, Mulinyawe SB, Annis DS, Huberman AD, et al. Gabapentin receptor alpha2delta-1 is a neuronal thrombospondin receptor responsible for excitatory CNS synaptogenesis. Cell. 2009; 139:380–392. [PubMed: 19818485]

Finney EM, Stone JR, Shatz CJ. Major glutamatergic projection from subplate into visual cortex during development. The Journal of comparative neurology. 1998; 398:105–118. [PubMed: 9703030]

Gabernet L, Jadhav SP, Feldman DE, Carandini M, Scanziani M. Somatosensory integration controlled by dynamic thalamocortical feed-forward inhibition. Neuron. 2005; 48:315–327. [PubMed: 16242411]

Gil Z, Connors BW, Amitai Y. Efficacy of thalamocortical and intracortical synaptic connections: quanta, innervation, and reliability. Neuron. 1999; 23:385–397. [PubMed: 10399943]

Goda Y, Davis GW. Mechanisms of synapse assembly and disassembly. Neuron. 2003; 40:243–264. [PubMed: 14556707]

Hanganu IL, Kilb W, Luhmann HJ. Functional synaptic projections onto subplate neurons in neonatal rat somatosensory cortex. J Neurosci. 2002; 22:7165–7176. [PubMed: 12177212]

Hu H, Cavendish JZ, Agmon A. Not all that glitters is gold: off-target recombination in the somatostatin-IRES-Cre mouse line labels a subset of fast-spiking interneurons. Frontiers in neural circuits. 2013; 7:195. [PubMed: 24339803]

Jiao Y, Zhang C, Yanagawa Y, Sun QQ. Major effects of sensory experiences on the neocortical inhibitory circuits. J Neurosci. 2006; 26:8691–8701. [PubMed: 16928857]

Kanold PO, Luhmann HJ. The subplate and early cortical circuits. Annual review of neuroscience. 2010; 33:23–48.

Kapfer C, Glickfeld LL, Atallah BV, Scanziani M. Supralinear increase of recurrent inhibition during sparse activity in the somatosensory cortex. Nat Neurosci. 2007; 10:743–753. [PubMed: 17515899]

Karayannis T, Au E, Patel JC, Kruglikov I, Markx S, Delorme R, Heron D, Salomon D, Glessner J, Restituito S, et al. Cntnap4 differentially contributes to GABAergic and dopaminergic synaptic transmission. Nature. 2014; 511:236–240. [PubMed: 24870235]

Kepecs A, Fishell G. Interneuron cell types are fit to function. Nature. 2014; 505:318–326. [PubMed: 24429630]

Kruglikov I, Rudy B. Perisomatic GABA release and thalamocortical integration onto neocortical excitatory cells are regulated by neuromodulators. Neuron. 2008; 58:911–924. [PubMed: 18579081]

Lazarus MS, Huang ZJ. Distinct maturation profiles of perisomatic and dendritic targeting GABAergic interneurons in the mouse primary visual cortex during the critical period of ocular dominance plasticity. Journal of neurophysiology. 2011; 106:775–787. [PubMed: 21613595]

Li Y, Stam FJ, Aimone JB, Goulding M, Callaway EM, Gage FH. Molecular layer perforant path-associated cells contribute to feed-forward inhibition in the adult dentate gyrus. Proceedings of the National Academy of Sciences of the United States of America. 2013; 110:9106–9111. [PubMed: 23671081]

Long MA, Cruikshank SJ, Jutras MJ, Connors BW. Abrupt maturation of a spike-synchronizing mechanism in neocortex. J Neurosci. 2005; 25:7309–7316. [PubMed: 16093380]

Luhmann HJ, Prince DA. Postnatal maturation of the GABAergic system in rat neocortex. Journal of neurophysiology. 1991; 65:247–263. [PubMed: 1673153]

Ma Y, Hu H, Berrebi AS, Mathers PH, Agmon A. Distinct subtypes of somatostatin-containing neocortical interneurons revealed in transgenic mice. J Neurosci. 2006; 26:5069–5082. [PubMed: 16687498]

Marin O. Interneuron dysfunction in psychiatric disorders. Nature reviews Neuroscience. 2012; 13:107–120. [PubMed: 22251963]

Minlebaev M, Colonnese M, Tsintsadze T, Sirota A, Khazipov R. Early gamma oscillations synchronize developing thalamus and cortex. Science. 2011; 334:226–229. [PubMed: 21998388]

Miyoshi G, Butt SJ, Takebayashi H, Fishell G. Physiologically distinct temporal cohorts of cortical interneurons arise from telencephalic Olig2-expressing precursors. J Neurosci. 2007; 27:7786–7798. [PubMed: 17634372]

Miyoshi G, Fishell G. GABAergic interneuron lineages selectively sort into specific cortical layers during early postnatal development. Cereb Cortex. 2011; 21:845–852. [PubMed: 20732898]

Molnar Z, Clowry G. Cerebral cortical development in rodents and primates. Progress in brain research. 2012; 195:45–70. [PubMed: 22230622]

Molnar Z, Kurotani T, Higashi S, Yamamoto N, Toyama K. Development of functional thalamocortical synapses studied with current source-density analysis in whole forebrain slices in the rat. Brain research bulletin. 2003; 60:355–371. [PubMed: 12781324]

Morales B, Choi SY, Kirkwood A. Dark rearing alters the development of GABAergic transmission in visual cortex. The Journal of neuroscience: the official journal of the Society for Neuroscience. 2002; 22:8084–8090. [PubMed: 12223562]

Narboux-Neme N, Evrard A, Ferezou I, Erzurumlu RS, Kaeser PS, Laine J, Rossier J, Ropert N, Sudhof TC, Gaspar P. Neurotransmitter release at the thalamocortical synapse instructs barrel formation but not axon patterning in the somatosensory cortex. J Neurosci. 2012; 32:6183–6196. [PubMed: 22553025]

Nery S, Fishell G, Corbin JG. The caudal ganglionic eminence is a source of distinct cortical and subcortical cell populations. Nat Neurosci. 2002; 5:1279–1287. [PubMed: 12411960]

Neske GT, Patrick SL, Connors BW. Contributions of diverse excitatory and inhibitory neurons to recurrent network activity in cerebral cortex. J Neurosci. 2015; 35:1089–1105. [PubMed: 25609625]

Osakada F, Mori T, Cetin AH, Marshel JH, Virgen B, Callaway EM. New rabies virus variants for monitoring and manipulating activity and gene expression in defined neural circuits. Neuron. 2011; 71:617–631. [PubMed: 21867879]

Owen SF, Tuncdemir SN, Bader PL, Tirko NN, Fishell G, Tsien RW. Oxytocin enhances hippocampal spike transmission by modulating fast-spiking interneurons. Nature. 2013; 500:458–462. [PubMed: 23913275]

Owens DF, Kriegstein AR. Is there more to GABA than synaptic inhibition? Nature reviews Neuroscience. 2002; 3:715–727. [PubMed: 12209120]

Pangratz-Fuehrer S, Hestrin S. Synaptogenesis of electrical and GABAergic synapses of fast-spiking inhibitory neurons in the neocortex. J Neurosci. 2011; 31:10767–10775. [PubMed: 21795529]

Petilla Interneuron Nomenclature, G. Ascoli GA, Alonso-Nanclares L, Anderson SA, Barrionuevo G, Benavides-Piccione R, Burkhalter A, Buzsaki G, Cauli B, Defelipe J, et al. Petilla terminology: nomenclature of features of GABAergic interneurons of the cerebral cortex. Nature reviews Neuroscience. 2008; 9:557–568. [PubMed: 18568015]

Petreanu L, Mao T, Sternson SM, Svoboda K. The subcellular organization of neocortical excitatory connections. Nature. 2009; 457:1142–1145. [PubMed: 19151697]

Pfeffer CK, Xue M, He M, Huang ZJ, Scanziani M. Inhibition of inhibition in visual cortex: the logic of connections between molecularly distinct interneurons. Nat Neurosci. 2013; 16:1068–1076. [PubMed: 23817549]

Picardo MA, Guigue P, Bonifazi P, Batista-Brito R, Allene C, Ribas A, Fishell G, Baude A, Cossart R. Pioneer GABA Cells Comprise a Subpopulation of Hub Neurons in the Developing Hippocampus. Neuron. 2011; 71:695–709. [PubMed: 21867885]

Represa A, Ben-Ari Y. Trophic actions of GABA on neuronal development. Trends in neurosciences. 2005; 28:278–283. [PubMed: 15927682]

Rudy B, Fishell G, Lee S, Hjerling-Leffler J. Three groups of interneurons account for nearly 100% of neocortical GABAergic neurons. Dev Neurobiol. 2011; 71:45–61. [PubMed: 21154909]

Sauer JF, Bartos M. Recruitment of early postnatal parvalbumin-positive hippocampal interneurons by GABAergic excitation. J Neurosci. 2010; 30:110–115. [PubMed: 20053893]

Seidler B, Schmidt A, Mayr U, Nakhai H, Schmid RM, Schneider G, Saur D. A Cre-loxP-based mouse model for conditional somatic gene expression and knockdown in vivo by using avian retroviral vectors. Proceedings of the National Academy of Sciences of the United States of America. 2008; 105:10137–10142. [PubMed: 18621715]

Silberberg G, Markram H. Disynaptic inhibition between neocortical pyramidal cells mediated by Martinotti cells. Neuron. 2007; 53:735–746. [PubMed: 17329212]

Sousa VH, Miyoshi G, Hjerling-Leffler J, Karayannis T, Fishell G. Characterization of Nkx6-2-derived neocortical interneuron lineages. Cereb Cortex. 2009; 19(Suppl 1):i1–10. [PubMed: 19363146]

Southwell DG, Paredes MF, Galvao RP, Jones DL, Froemke RC, Sebe JY, Alfaro-Cervello C, Tang Y, Garcia-Verdugo JM, Rubenstein JL, et al. Intrinsically determined cell death of developing cortical interneurons. Nature. 2012; 491:109–113. [PubMed: 23041929]

Sun Y, Nguyen AQ, Nguyen JP, Le L, Saur D, Choi J, Callaway EM, Xu X. Cell-type-specific circuit connectivity of hippocampal CA1 revealed through Cre-dependent rabies tracing. Cell reports. 2014; 7:269–280. [PubMed: 24656815]

Takesian AE, Kotak VC, Sharma N, Sanes DH. Hearing loss differentially affects thalamic drive to two cortical interneuron subtypes. Journal of neurophysiology. 2013; 110:999–1008. [PubMed: 23719211]

Taniguchi H, He M, Wu P, Kim S, Paik R, Sugino K, Kvitsiani D, Fu Y, Lu J, Lin Y, et al. A resource of Cre driver lines for genetic targeting of GABAergic neurons in cerebral cortex. Neuron. 2011; 71:995–1013. [PubMed: 21943598]

Tong Q, Ye CP, Jones JE, Elmquist JK, Lowell BB. Synaptic release of GABA by AgRP neurons is required for normal regulation of energy balance. Nat Neurosci. 2008; 11:998–1000. [PubMed: 19160495]

Tuncdemir SN, Fishell G, Batista-Brito R. miRNAs are Essential for the Survival and Maturation of Cortical Interneurons. Cereb Cortex. 2015; 25:1842–1857. [PubMed: 24451661]

Wickersham IR, Lyon DC, Barnard RJ, Mori T, Finke S, Conzelmann KK, Young JA, Callaway EM. Monosynaptic restriction of transsynaptic tracing from single, genetically targeted neurons. Neuron. 2007; 53:639–647. [PubMed: 17329205]

Williams ME, de Wit J, Ghosh A. Molecular mechanisms of synaptic specificity in developing neural circuits. Neuron. 2010; 68:9–18. [PubMed: 20920787]

Wonders CP, Anderson SA. The origin and specification of cortical interneurons. Nature reviews Neuroscience. 2006; 7:687–696. [PubMed: 16883309]

Xu H, Jeong HY, Tremblay R, Rudy B. Neocortical somatostatin-expressing GABAergic interneurons disinhibit the thalamorecipient layer 4. Neuron. 2013; 77:155–167. [PubMed: 23312523]

Zhang Y, Narayan S, Geiman E, Lanuza GM, Velasquez T, Shanks B, Akay T, Dyck J, Pearson K, Gosgnach S, et al. V3 spinal neurons establish a robust and balanced locomotor rhythm during walking. Neuron. 2008; 60:84–96. [PubMed: 18940590]

Zhang ZW. Maturation of layer V pyramidal neurons in the rat prefrontal cortex: intrinsic properties and synaptic function. Journal of neurophysiology. 2004; 91:1171–1182. [PubMed: 14602839]

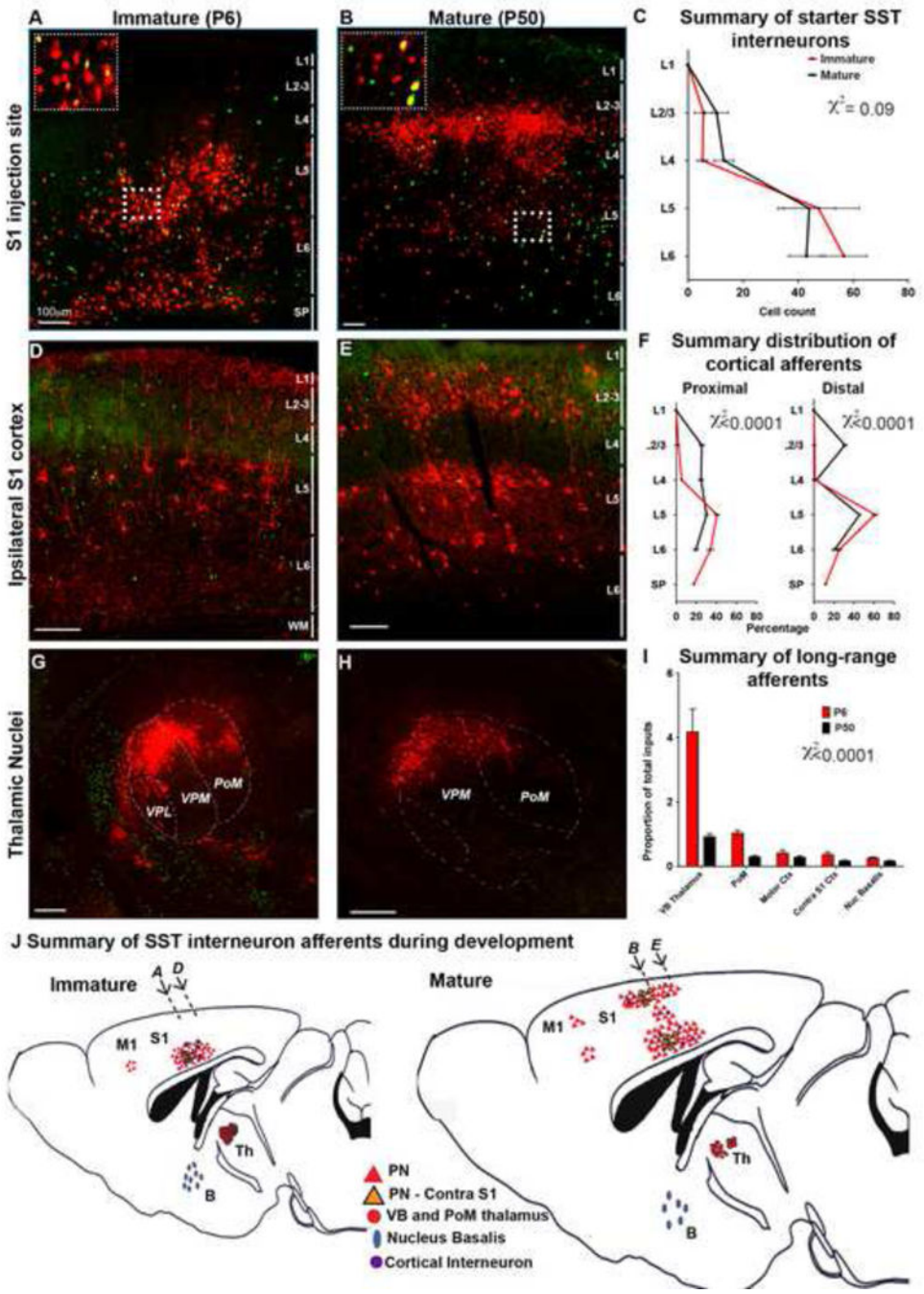

Figure 1. SST interneurons undergo reorganization in their afferent connectivity during development

Representative images of the injection site in S1BC at P6 (A) and P50 (B) insets show higher magnification image of the SST neurons (green), starter neurons (yellow), and their presynaptic partners (red) in L5 (C) Starter neurons in immature (P6, n=5) and mature (P30, n=2, P50, n=5) animals predominantly localized in L5 and 6 with only a minority of the starter neurons in L2/3 and L4 that did not show statistically significant differences across two developmental stage (χ^2=0.09). See also Table S1. (D) At P6 retrogradely labeled (mCh^+) neurons found primarily in deep layers of ipsilateral cortex 300μm caudal to

injection site. (E) Reorganization of presynaptic neurons at P50 in upper and deeper layers 300μm caudal to injection site. (F) The distribution of cortical inputs 150μm (left) and 300μm R-C (right) to the injection site. Data represents the averaged percentage of presynaptic neurons in a layer within the entire cortex ipsilateral to the injection site (χ^2<0.001). (G) Subcortical afferent projections from ventrobasal (VB) and PoM nucleus of the thalamus at P6. (H) Thalamic inputs showed a reduction in older animals. (I) Proportion of presynaptic neurons projected from long-range regions, data represents the number of presynaptic neurons normalized to number of starter neurons in counted in 1/6th of brains. Long range afferents onto SST interneurons showed a statistically significant dependence on developmental stage (χ^2<0.001). Mean ± SEM, Pearson's chi-square test, scale bars 100μm, see also Figure S1. (J) Summary of SST interneuron afferents during development, arrows correspond to image locations in A, B, D and E.

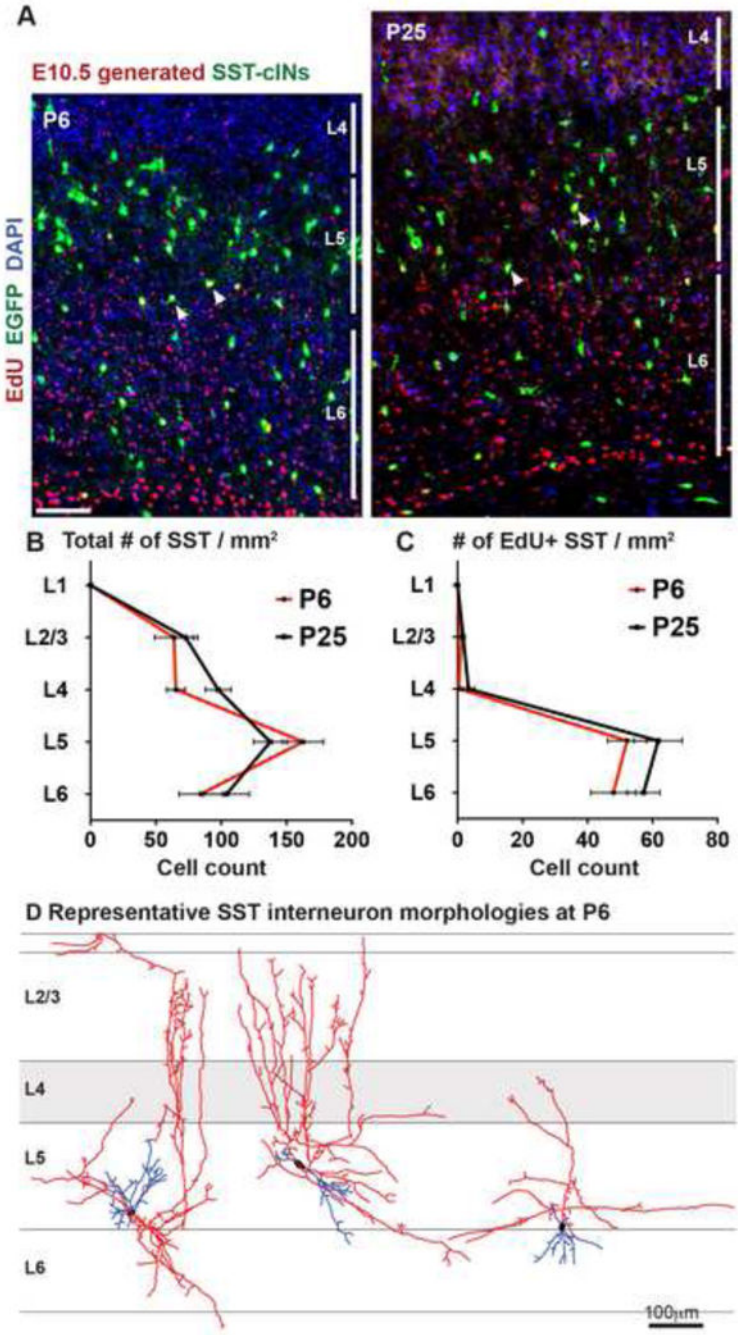

Figure 2. Changes in SST interneuron afferent connectivity do not result from changes in the L5/6 population

(A) Genetically labeled SST interneurons born at E10.5 are saturation labelled with EdU and the number of SST interneurons were assessed at P6 (left) and and P25 (right). (B) The density of $EGFP^+$ SST interneurons in per mm^2 of each layer within infragranular layers of S1BC does not change when normalized to the brain volume at P6 and P25 ($p>0.05$) (C) The number of SST interneurons generated at E10.5 (EdU^+EGFP^+ doubled labeled cells) at P6 were not significantly different compared to P25 ($p>0.05$). n=3 animals, $n \geq 3$ sections were analyzed per animal, mean ± SEM, two-sample t-test, scale bars 50µm, see also Figure S2.

(D) Exemplary SST interneuron reconstructions at P6 obtained by diluted EnvA+RV*dG*-mCh injections into SST^{CRE}; Rosa-TVA mice displays heterogeneous morphological arborizations.

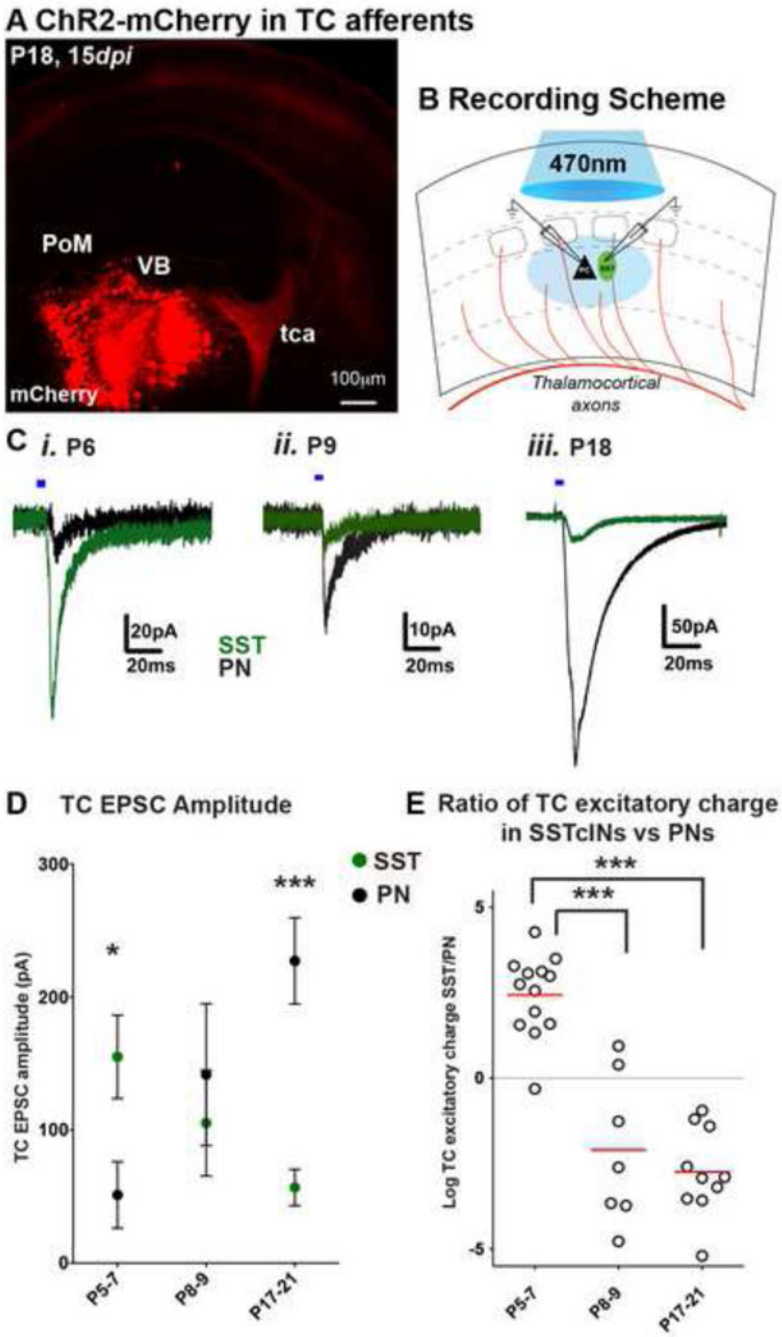

Figure 3. Functional monosynaptic thalamocortical inputs on SST interneurons are rapidly reduced after the first postnatal week

(A) AAV-ChR2-mCh injected on E14.5 or P1–3 to target thalamocortical afferents and examined 7–15 days later (See Figure S2). (B) Recording configuration for analyzing EPSCs from SST interneurons and adjacent PNs in the L5A/6B of barrel cortex. (C) Representative traces of light evoked thalamic EPSCs recorded at −65mV holding potential, in the presence of TTX (1μM) and 4-AP (800μM) from adjacently localized SST interneuron (green), and PN (black) EPSCs at P6, P9 and P18. Blue horizontal bars represent photostimulation (470nm, 5ms, 0.5 mW). Note that the amplitude of events are smaller in

P8–9 intermediate time points due to shorter expression time of ChR2 (AAV injection on P1, recording 7–8 days post infection, *dpi*) compared to amplitude of events at P6 (11 *dpi*) or P18 (15 *dpi*) (D) Averaged TC EPSC amplitudes (pA) show P5–7 SST interneuron received stronger inputs compared to PNs ($n=13$, $p<0.05$); while the inputs were similar at P8–9 ($n=7$, $p>0.05$), SST interneuron inputs were significantly smaller than PN inputs at P17–21 ($n=11$, mean ± SEM, $p<0.0001$). (E) Log2 normalized ratio of excitatory charges (pC) recorded on SST interneurons and PNs show a dramatic reduction by the end of 1st postnatal week. SST interneuron vs PN charge ratio compared to both P8–9, and P17–21 ($p<0.0001$). For each time point, $n \geq 3$ animals, $n \geq 2$ brain slices were analyzed per animal, Mann-Whitney test, see also Figure S3 and Table S2.

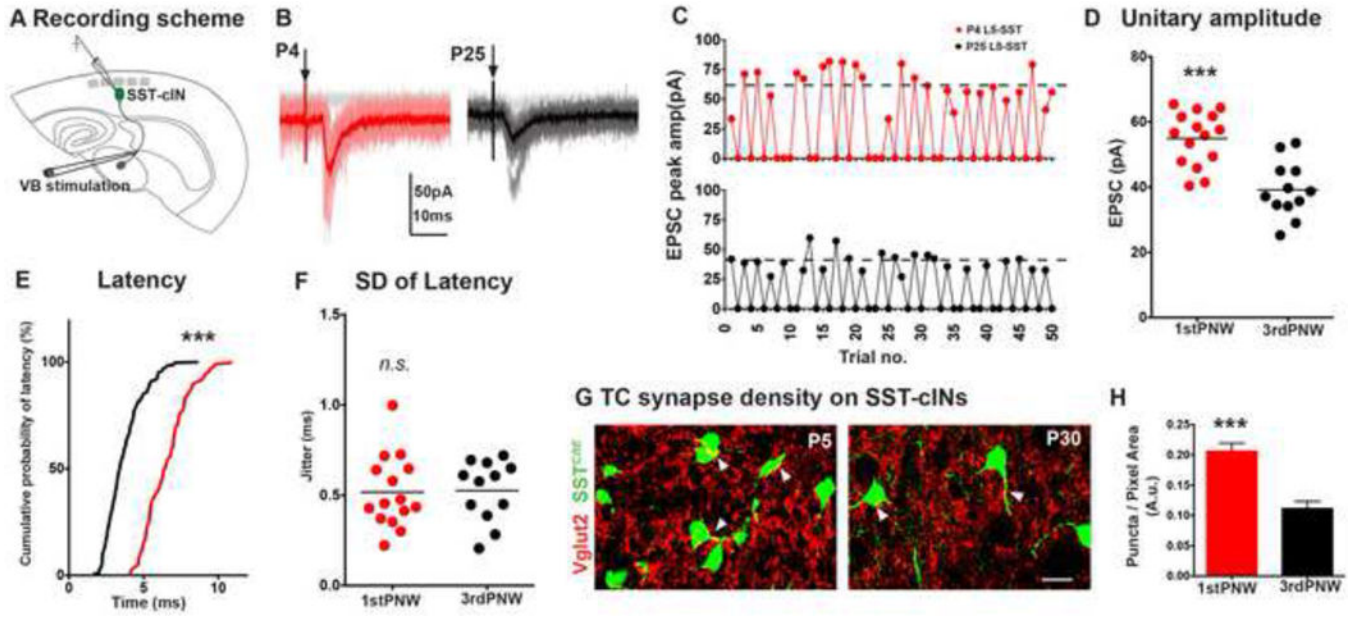

Figure 4. Thalamic excitation of SST interneurons is reduced during development

(A) Synaptic events in SST interneurons recorded from L5B/L6A in a TC slice preparation at P3–6 and P20–25 using minimal stimulation protocol (50–500μA) to evoke EPSCs only in half of the trials. (B) Representative traces of TC-EPSCs in P4 (red) and P25 (black) SST interneurons. (C) Exemplary recording sessions showing distribution of minimal events during 50 sweeps, dashed lines represent the averaged potency. (D) Excluding failures, peak TC EPSCs in SST interneurons of immature brains (n=15) showed a small but significant improvement over mature SST interneurons than those of older mice (n=12, $p<0.0001$, Mann-Whitney test) (E). Thalamic EPSC latency was longer in immature mice, relative to older animals ($p<0.0001$, Kolmogorov-Smirnov test). (F) Mean standard deviation of latency was not significantly different between two ages ($p>0.05$, Mann-Whitney test). For each time point, $n \geq 4$ animals, $n \geq 2$ brain slices were analyzed per animal. See also Figure S4. (G) Vglut2 immunoflouroscence in genetically identified P5 (left), and P30 SST interneurons (right). Images are pseudocolored for clarity, scale bar corresponds to 10μm. (H) Vglut2 synaptic puncta density on SST interneurons were significantly larger in P5 animals compared to older animals ($p<0.0001$). $n \geq 9$ areas analyzed from $n \geq 10$ cells, 3 animals, 3 sections per animal, mean ± SEM, Mann-Whitney test.

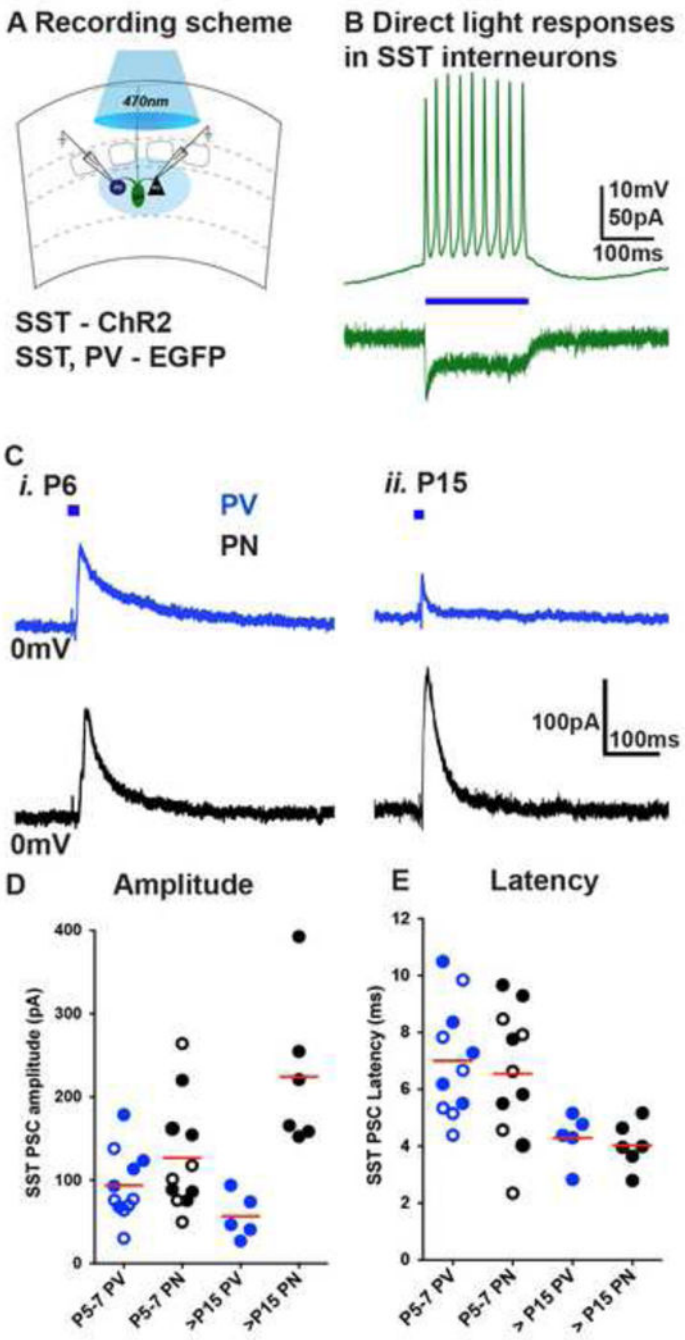

Figure 5. Immature SST interneurons broadly innervate deep cortical layers

(A) ChR2 was targeted to SST interneurons by SST^{CRE}; Ai32$^{ChR2\text{-}EYFP}$; Lhx6^{EGFP} mouse line or AAV-flex-hChR2.mCherry virus injections into infragranular layers of SST^{CRE}; Lhx6^{EGFP} mice and synaptic currents in Lhx6^{EGFP} positive PV interneurons and adjacent PNs in the L5A/6B of barrel cortex recorded at 0mV holding potential, in the presence of NBQX (10μM) and DAP-5 (25μM). (B) Light (blue horizontal bar, 100ms) induced responses in SST interneurons. (C) Representative traces of SST interneuron evoked responses (5ms light pulses) in PV interneurons (blue) and PNs. (D) Representative

fluorescent image of a P6 coronal slice containing ChR2-mCherry expressing SST interneurons 5 days after AAV-flex-hChR2.mCherry virus injections into infragranular layers of SST^{CRE}; $Lhx6^{EGFP}$ mice. (E) Light evoked synaptic currents at P6 in $Lhx6^{EGFP}$ positive PV interneurons and adjacent PNs in the L5A/6B of barrel cortex recorded at 0mV holding potential, in the presence of NBQX (10μM) and DAP-5 (25μM), blue horizontal bar indicates 10ms light pulse. (F) SST-PSC amplitudes in PV interneuron (transgenic closed circles, n=5; virus open circles, n=6) were similar in PNs (transgenic closed circles, n=6; virus open circles, n=5) at P5–6 ($p>0.05$), while PV interneuron (transgenic, n=5) were significantly smaller than PNs (transgenic, n=6) at P15–18 ($p<0.0001$). G) Latency of light-evoked IPSCs (ms) were similar among PV interneurons and PNs ($p>0.05$). For each time point, n=2 animals, n=2 brain slices were analyzed per animal, Mann-Whitney test

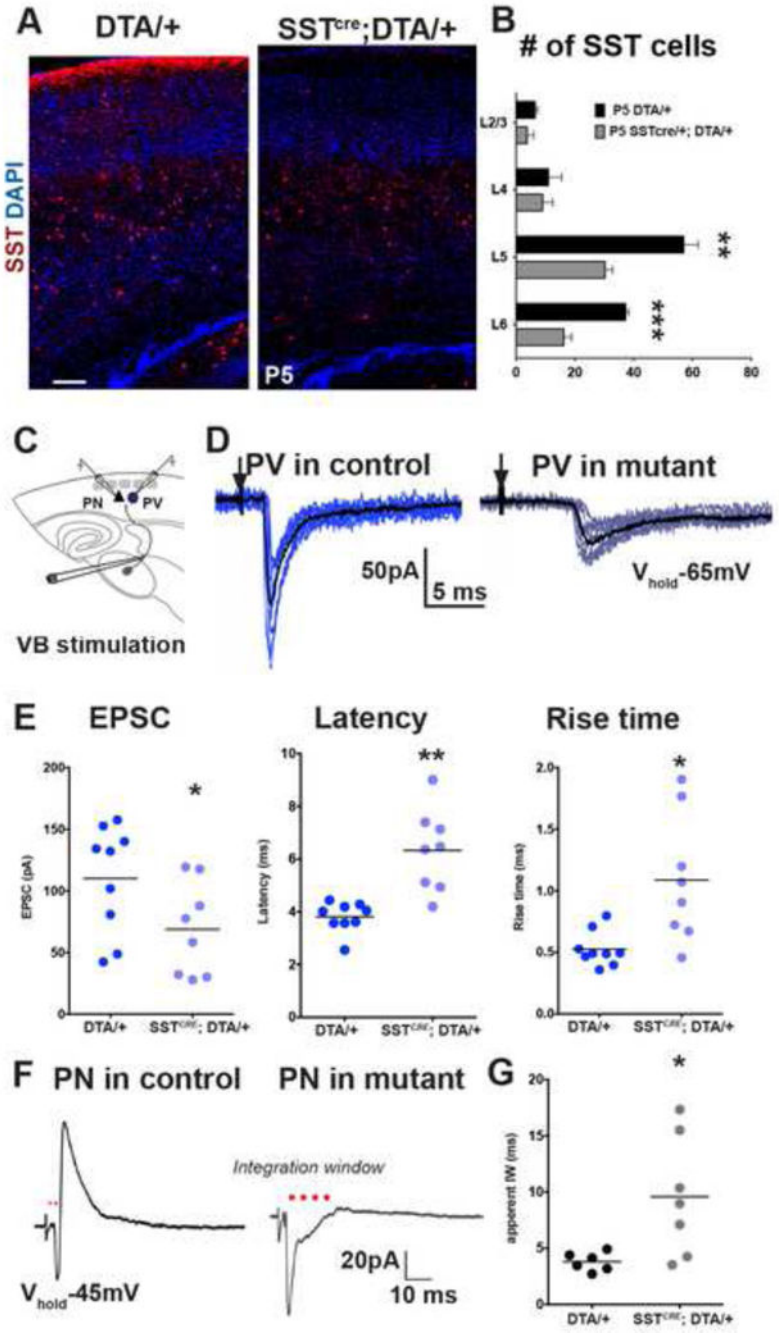

Figure 6. Ablation SST interneuron during early development leads to an arrest in PV interneuron input maturation

(A) SST immunoflouroscence in Rosa-DTA$^{loxp/+}$ (left panel) and SST^{CRE}; Rosa-DTA$^{loxp/+}$ (right panel). (B) SST interneuron numbers were significantly different in L5 and L6 in mutant animals compared to controls ($p<0.001$). N=3 mutant, n=4 control, n≥3 coronal sections were analyzed per animal, mean ± SEM, two-sample t-test. (C) Recording scheme. (D) Representative traces of unitary TC EPSCs in Lhx6^{EGFP} positive PV interneurons in aged matched Rosa-DTA$^{loxp/+}$ controls (dark blue, left) and SST^{CRE}; Rosa-DTA$^{loxp/+}$ mutants (light blue, right) (stimulation intensity, 75 μA). (E) Evoked TC responses in PV

interneurons in controls (n=9, 2 animals, 3 slices), and mutants (n=8, 2 animals, 4 slices) recorded between P10–12 showed significant differences in averaged peak amplitude (left, $p<0.05$), latency (middle, $p<0.01$), and rise time (right, $p<0.05$). (F) Representative traces of averaged EPSC-IPSC sequences in L5/6 PNs in control (left) and mutant animals (right) evoked by TC fiber stimulation at −45mV holding potential. (G) Population data representing the averaged integration window (IW, marked by red dots) in controls (n=6), and mutants (n=7, $p<0.05$). Mann-Whitney test, see also Figure S6.

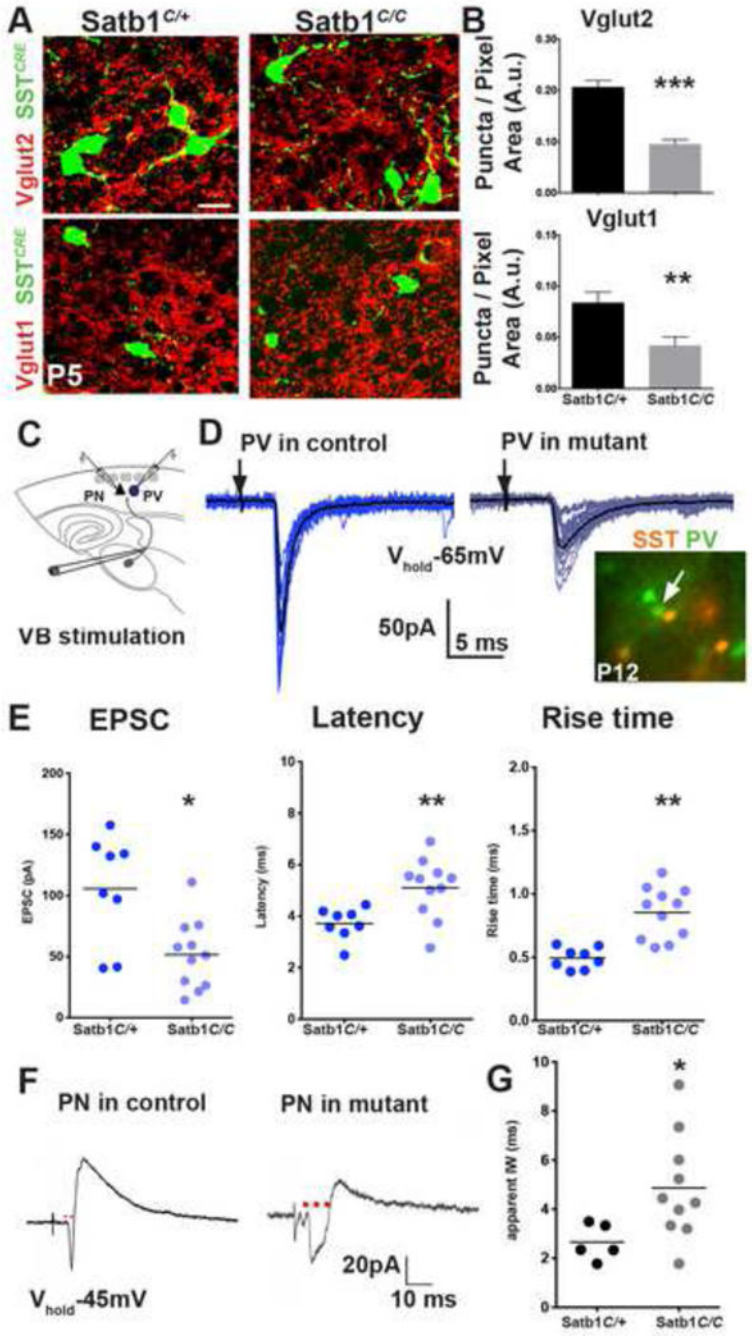

Figure 7. *Satb1* loss of function in SST interneurons leads to an arrest in PV interneuron input maturation

(A) Vglut2 (top), and Vglut1 (bottom) immunoflouroscence in genetically identified P5 Satb1$^{C/+}$ control (left), and Satb1$^{C/C}$ mutant (right) SST interneurons. Scale bar corresponds to 10μm. (B) Vglut2 (top), and Vglut1 (bottom) synaptic puncta density on SST interneurons were significantly larger in controls compared to mutant animals (n≥10 areas analyzed from n≥12 cells, 3 animals, 3 sections per animal, mean ± SEM, p<0.0001, two-sample t-test). (C) Recording scheme. (D) Representative traces of EPSCs in PV interneurons in aged matched SST^{CRE}; Rosa-Ai9^{tdTomato}; Satb1$^{C/+}$ controls (P12, dark blue, left) and SST^{CRE}; Rosa-

Ai9^{tdTomato}; Satb1$^{C/C}$ mutants (P13, light blue, right) evoked by TC fiber stimulation at threshold (100 μA), bottom right image shows the Lhx6^{EGFP} positive, Rosa-Ai9^{tdTomato} negative cells targeted for recording. (E) Evoked TC responses in PV interneurons in controls (n=8, 2 animals, 3 slices), and mutants (n=11, 3 animals, 4 slices) recorded between P11–14 showed significant differences in averaged peak amplitude (left, $p<0.05$), latency (middle, $p<0.01$), and rise time (right, $p<0.01$). (F) Representative traces of averaged EPSC-IPSC sequences in L5/6 PNs in control (left) and mutant animals (right) evoked by TC fiber stimulation at −45mV holding potential. (G) Population data representing the averaged IW (red dots) in controls (n=5, 2 animals, 3 slices), and mutants (n=10, 3 animals, 5 slices, $p<0.05$). Mann-Whitney test, see also Figure S7.

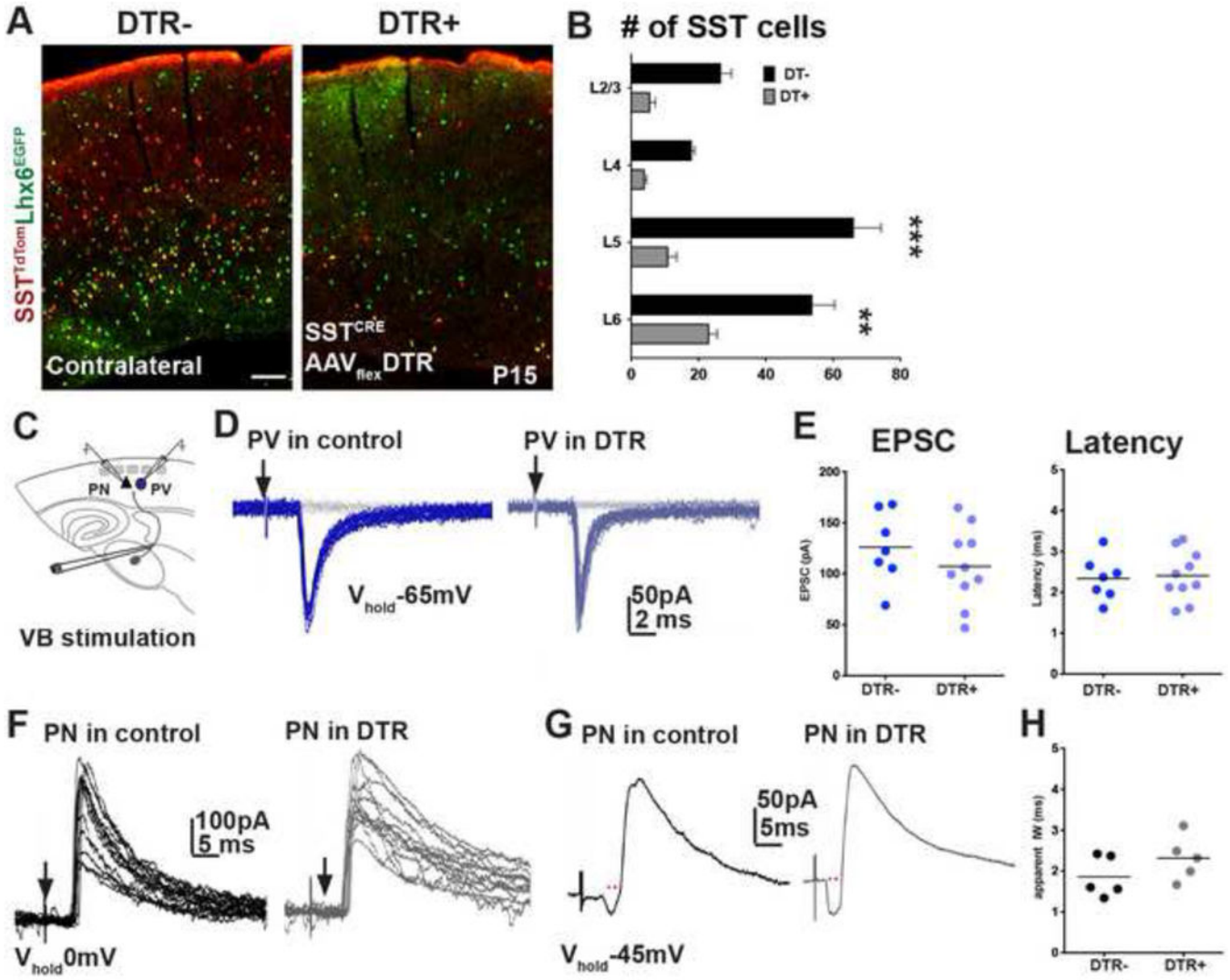

Figure 8. Ablation SST interneuron network after second postnatal week do not affect TC inputs onto PV interneurons

(A) TdTomato and EGFP flourescence in AAV-flex-DTR.GFP injected (right) and contralateral (left) hemispheres of $SST^{CRE};Ai9^{TdTomato};Lhx6^{EGFP}$ animals. (B) Selective expression of DT in $SST^{CRE};Ai9^{TdTomato}$ neurons after the first postnatal week leads to a significant reduction in the number in virus injected hemispheres compared contralateral side in all cortical layers (n=3, mean ± SEM, $p<0.001$, two-sample t-test). (C) Recording scheme. (D) Representative traces of unitary TC EPSCs in $Lhx6^{EGFP}$ positive PV interneurons in contralateral (dark blue, left) and AAV expressing mutants (light blue, right) hemispheres (stimulation intensity, 75 μA). (E) Evoked TC responses in PV interneurons in controls (n=10, 4 animals, 6 slices), and mutants (n=7, 4 animals, 4 slices) recorded between P13–17 did not show significant differences in averaged peak amplitude (left, p=0.26) or latency (right, p=0.78). (F) Overlay of IPSCs (V_{hold} = 0mV) recorded in PNs in control (left) and mutant (right) hemispheres. (G) Representative traces of IPSC sequences in L5/6 PNs in control (left) and mutant hemispheres (right) evoked by TC fiber stimulation at −45mV

holding potential. (H) Averaged IW (red dots in G) in controls (n=5), and mutants (n=5, p=0.22). Mann-Whitney test.